Journal of Advanced Ceramics
2014, 3(3): 215–223
DOI: 10.1007/s40145-014-0112-2

ISSN 2226-4108
CN 10-1154/TQ

Research Article

Frequency dependent electrical properties of $Na_2Pb_2R_2W_2Ti_4Nb_4O_{30}$ (R = Nd, Sm) ceramics

Lalatendu BISWAL[a,c], Piyush R. DAS[b,*], Banarji BEHERA[c]

[a]*Department of Physics*, *SOT*, *KIIT University, Bhubaneswar-751024*, *Odisha*, *India*
[b]*Department of Physics*, *Veer Surendra Sai University of Technology*, *Burla-768018*, *Sambalpur*, *India*
[c]*School of Physics*, *Sambalpur University*, *Jyoti Vihar*, *Burla-768019*, *Odisha*, *India*

Received: March 15, 2014; Revised: June 09, 2014; Accepted: June 12, 2014

Abstract: In the present research work, frequency dependent electrical properties of tungsten bronze structured compounds $Na_2Pb_2R_2W_2Ti_4Nb_4O_{30}$ (R = Nd, Sm) are reported. X-ray diffraction (XRD) study of polycrystalline ceramic samples confirms the formation of compounds with orthorhombic structure. Analysis of frequency dependent electrical data in the framework of modulus and conductivity formalism suggests the presence of thermally activated relaxation process in the compounds, which show Arrhenius behavior. The magnitudes of activation energies give the nature of the relaxing species. The real and imaginary parts of complex modulus trace the depressed semicircle in complex plane, suggesting non-Debye type relaxation process in the materials. The power law behavior of admittance data is successfully modeled by introducing constant phase element (CPE) to the equivalent circuit. A large value of power law parameter (n) of CPE below ferroelectric transition temperature (T_c) is attributed to the cooperative response of the dipoles which is reduced above T_c. This behavior is correlated with the frequency dependence of CPE, suggesting a physical meaning to it. The frequency dependent AC conductivity at different temperatures follows Jonscher's universal power law. Almond and West formalism is used to estimate the hopping rate, activation enthalpy and charge carrier concentration in the materials.

Keywords: ceramics; electrical properties; microstructure; electrical conductivity

1 Introduction

Interest on tungsten bronze structured dielectric ceramics in polycrystalline or single crystal form has increased considerably because of their interesting properties for device applications [1–6]. The general chemical formula for these materials is $[(A_1)_2(A_2)_4(C)_4][(B_1)_2(B_2)_8]O_{30}$, consisting complex array of distorted BO_6 octahedra sharing corners providing three different interstices (A_1, A_2, B_1, B_2 and C) for cation substitution. Due to the complex structure, its physical properties can be tailored through suitable cation substitutions, but these physical properties are also dependent on the synthesis route, environment and time of formation. The electrical properties basically depend on the physical processes that go on within the material when it is stimulated to external perturbations. Identifying the physical processes and estimating the contribution of microstructures of the material to these electrical processes are a great task to the researchers. A complete knowledge about these helps one to select the cations to be substituted and conditions of

* Corresponding author.
E-mail: prdas63@gmail.com, prdas@iter.ac.in

formation for its suitability in device applications.

Complex impedance spectroscopy (CIS) technique has been widely used to investigate the physical processes deciding the electrical properties of dielectric materials, electrochemical systems and their interfaces with electronic conducting electrodes. It helps to separate grain (intragrain) and grain boundary (intergrain) contributions in transport properties of the materials [7]. In this technique, the system under study is exposed to small sinusoidal AC of variable frequency at different temperatures and the corresponding impedance is measured. The variation of impedance parameters with frequency and temperature can be suitably modeled with equivalent circuits, which helps the investigator in identifying the responsible physical processes [8]. Once the equivalent circuit is selected correctly, the contribution of different electrical active regions in the material can be separated from the total impedance, and hence a complete knowledge of the electrical microstructure of the material can be obtained. In CIS technique, the AC response of the polycrystalline dielectric ceramics has been analyzed in four different formalisms: (I) dielectric permittivity spectroscopy, (II) impedance spectroscopy, (III) modulus spectroscopy and (IV) admittance spectroscopy. Though all these formalisms are intimately related with each other, they are equally important because of their different dependence and weight with frequency. For the polycrystalline dielectric samples whose conductivity is not very low, both complex impedance spectroscopy and modulus spectroscopy formalisms are adopted. Since the imaginary part of impedance (Z'') is proportional to bulk resistance and the imaginary part of modulus (M'') is inversely proportional to bulk capacitance, the impedance formalism emphasizes the inter granular conduction processes, whereas the electric modulus formalism is dominated by bulk effects [9].

The electrical properties of ferroelectric materials are found to be mostly frequency dependent (particularly at high frequency), which keep them away from ideal Debye-like behavior. This frequency dependence of electrical properties is attributed to the distribution of relaxation time. Jonscher [10] has suggested that the dispersion of impedance parameters is a universal property of dielectric materials, which is substantiated by theoretical works of Ngai and White [11] and Dissado and Hill [12]. Now it is well accepted that the dispersion is the consequence of many body interactions between the conducting species present in the material. Researchers take different approaches to model this non-ideality by modifying the functional form of impedance parameters through introduction of new circuit elements like constant phase elements (CPEs) [13]. The physical meaning of CPE is poorly understood [14]. Some researchers attribute CPE to the roughness of the electrode–electrolyte interfaces or to the inhomogenieties in the local distribution of defects in the vicinity of grain boundaries [15–17].

In this paper, we are reporting the frequency dependent electrical properties of polycrystalline ferroelectric ceramics $Na_2Pb_2R_2W_2Ti_4Nb_4O_{30}$ (R = Nd, Sm) through modulus spectroscopy, admittance spectroscopy and AC conductivity analysis. We have tried to suggest physical interpretation to CPE from the study of the frequency dependent electrical properties of the above compounds. The experimental procedure of synthesis, structural characterization and dielectric properties of above mentioned materials were reported earlier [18,19]. The structural study revealed the formation of polycrystalline samples of tungsten bronze type with orthorhombic structure. The materials were found to be ferroelectric in nature with transition temperature well above the room temperature (627 K for $Na_2Pb_2Sm_2W_2Ti_4Nb_4O_{30}$ (NPSWTN) and 567 K for $Na_2Pb_2Nd_2W_2Ti_4Ta_4O_{30}$ (NPNWTT)).

2 Experimental

Solid state reaction technique was adopted to prepare polycrystalline samples of $Na_2Pb_2R_2W_2Ti_4Nb_4O_{30}$ (R=Nd, Sm) (abbreviated as NPNWTN and NPSWTN, respectivley) using high purity (analytical reagent grade) ingredients Na_2CO_3, PbO, Sm_2O_3, Nd_2O_3, TiO_2, WO_3, and Nb_2O_5. These ingredients, taken in suitable stoichiometry, were thoroughly mixed and ground in dry and wet (methanol) medium each for 1 h in an agate and mortar. Calcinations were carried out at 1273 K for 4 h for both samples NPNWTN and NPSWTN. The processes of grinding and calcination were repeated to ensure the completion of the reaction. The quality and formation of the compounds were checked by X-ray diffraction (XRD) technique. Room temperature (298 K) XRD patterns of the compounds were obtained using an X-ray powder diffractometer (PHILIPS PW1817) with Cu Kα radiation (λ = 1.5418 Å) in a wide range of Bragg angle ($20° \leqslant 2\theta \leqslant 80°$) at a scanning rate of 3 (°)/min. The powder

was then pressed into pellets (10 mm in diameter and 1–2 mm in thickness) under a uniaxial pressure of 4×10^6 N/m^2. Polyvinyl alcohol (PVA) was used as binder to reduce the brittleness of the pellets. The binder was burnt out during the sintering. The pellets were then sintered at 1327 K for 4 h in air atmosphere. The sintered pellets were polished, coated with high purity conducting silver paste and then dried at 423 K for 4 h to remove the moisture. The electrical measurements of the pellets were carried out using a computer controlled Hioki 3532 LCR Hitester over a wide range of temperature.

3 Results and discussion

3.1 Electrical properties

The complex electric modulus formalism has been used to characterize the ionic conducting materials, because it can discriminate the electrical properties against the electrode polarization and other interfacial effects [9,20] and hence can be used to separate electrical active components with similar resistance but different capacitance. It is also used to analyze conductivity relaxation in the materials. Spectroscopic plots of imaginary parts of complex impedance and complex modulus may look very different for the materials, which are inhomogeneous and are represented by more than one RC element [21].

Figure 1 shows the variation of real part of electric modulus (M') of NPNWTN and NPSWTN as a function of frequency at various temperatures. For both the materials, M' has a very small value at low frequency and a continuous dispersion with frequency, and tends to an asymptotically saturation value at very high frequency. Very small value of M' at low frequency shows no contribution from electrode polarization. A continuous dispersion on increasing frequency is because of conductivity relaxation phenomenon, which is related to the lack of restoring force governing the mobility of charge carriers under the influence of steady electric field [22]. This is attributed to conduction due to short range mobility of charge carriers.

The spectroscopic plots of imaginary part of complex electric modulus (M'') for NPNWTN and NPSWTN are shown in Fig. 1 (insets). At a particular temperature, single peak in M'' vs. frequency plot

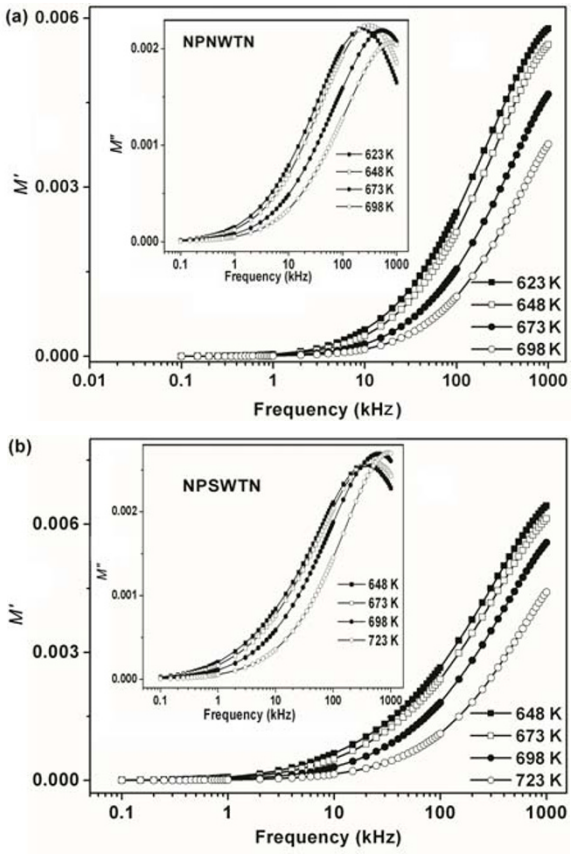

Fig. 1 Variations of real and imaginary parts of complex modulus with frequency for (a) NPNWTN and (b) NPSWTN.

can be seen. Appearance of the peak suggests conductivity relaxation phenomenon in the materials. The low frequency side of the peak gives the range of frequency at which the ions can move over long ranges, i.e., ions can perform successful hopping from one site to the neighboring site. The high frequency side of the peak gives the range of frequency at which the ions are confined to their potential wells and can have only localized motion within the wells [23,24].

As the temperature increases, the frequency peak of M'' shifts to high frequency side for both the materials. This shows that the relaxation process is thermally activated. The relaxation time for loss modulus spectrum is calculated using the relation $\tau = 1/(2\pi f_{\max})$. This relaxation time gives a measure of the time scale of transition from long range mobility [23]. Figure 2 gives the variation of this relaxation time with reciprocal temperature, which shows Arrhenius behavior. The activation energies obtained from Arrhenius plots are found to be 0.69 eV for

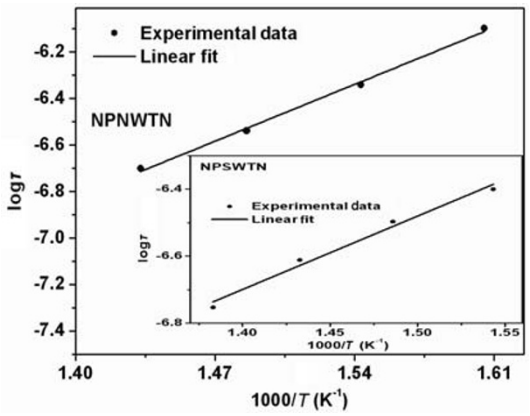

Fig. 2 Variation of relaxation time with temperature for NPNWTN and NPSWTN.

NPNWTN and 0.43 eV for NPSWTN. These values correspond to DC activation energy of the materials. These values of activation energy suggest that the DC conduction process is dominated by electrons and/or small polarons and defects (single oxygen ion vacancies).

Figure 3 gives the Nyquist plots of complex modulus for NPNWTN and NPSWTN at different temperatures. The curves do not form exact semicircles but possess a shape of deformed semicircle with their centers lying below *x*-axis. This shows a non-Debye type of relaxation in the materials having spread of relaxation with different time constants. Corresponding to a particular temperature, the modulus plane plot shows a single semicircle. The combined plots of loss modulus spectrum and loss impedance spectrum at temperatures 623 K for NPNWTN and 648 K for NPSWTN are shown in Fig. 3 (insets). The plots are made on log–log scale, instead of more commonly used linear–log scale in order to emphasize the departure from ideality [13]. The broad features, with the asymmetries and separations of peak maxima of the curves for both the materials, support the departure from ideal Debye-like behavior.

The depressed semicircles in the complex modulus plane and the non-coincidence of peaks in the frequency dependence of loss impedance and loss modulus spectra with peak asymmetries suggest that the frequency dependent electrical response of the compound cannot be modeled by an equivalent circuit consisting of resistance and capacitance only. This non-ideal behavior is attributed by many researchers to the phenomena taking place in the material with a spread of relaxation time due to the intrinsically dispersive nature of the material [9,25]. Jonscher [10]

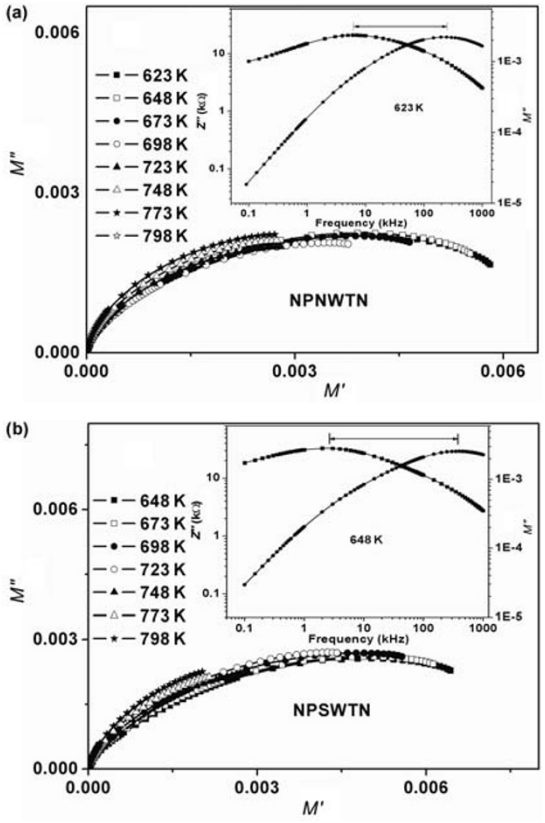

Fig. 3 Spectroscopic plots of complex modulus (real and imaginary parts) of (a) NPNWTN and (b) NPSWTN at different temperatures.

has suggested this dispersion to be a universal property of all dielectric materials and an inevitable consequence of many body interactions between the conducting species present in the material [9]. This intrinsically dispersive nature of the sample contributes to the bulk impedance behavior before the appearance of a second and separate contribution from the grain boundary impedance. To fit the data so obtained, a new circuit element, often called as constant phase element (CPE) is introduced and given by [26]:

$$Y_{\mathrm{CPE}} = 1/Z_{\mathrm{CPE}} = Y_0(\mathrm{j}\omega)^n \quad (1)$$

Then the equivalent circuit for bulk response consists of R–CPE–C in parallel.

The electrical response of polycrystalline samples at different temperatures can be modeled by an equivalent circuit consisting of a single RC circuit (at low temperatures) or a series of component circuits each containing parallel combination of resistance and capacitance [8] (at high temperatures). We have introduced CPE in the equivalent circuit for the bulk response (Fig. 4). Hence, electrical response at elevated temperature (< 573 K for both NPSWTN and

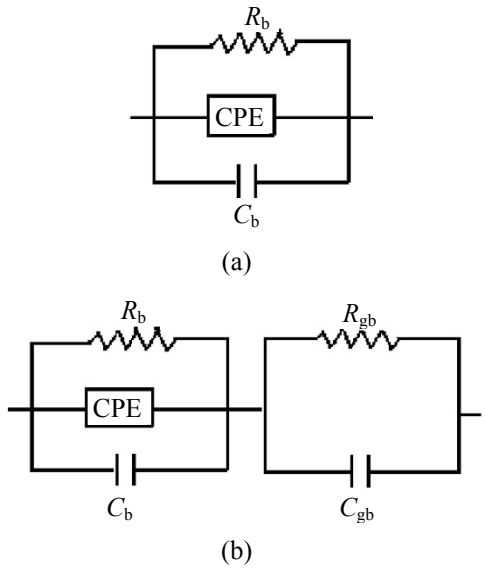

Fig. 4 Equivalent circuits for (a) bulk response alone and (b) bulk and grain boundary response.

NPNWTN) is modeled by (R–CPE–C) (Fig. 4(a)) and at moderately high temperature is modeled by (R–CPE–C)(R–C) (Fig.4(b)).

Then the impedance of the most general equivalent circuit (Fig. 4(b)), of which the other one is the special case (Fig. 4(a)), is given by

$$Z = [(1/R_b) + j\omega C_b + Y_0(j\omega)^n]^{-1} + [(1/R_{gb}) + j\omega C_{gb}]^{-1}$$

Substituting $j^n = \cos(n\pi/2) + j\sin(n\pi/2)$, $Y_0(j\omega)^n$ can be expanded as

$$Y_0(j\omega)^n = Y_0\omega^n[\cos(n\pi/2) + j\sin(n\pi/2)] = A\omega^n + jB\omega^n$$

So

$$\begin{aligned} Z &= [(1/R_b) + j\omega C_b + A\omega^n + jB\omega^n]^{-1} + [(1/R_{gb}) + j\omega C_{gb}]^{-1} \\ &= [(1/R_b) + A\omega^n + j(\omega C_b + B\omega^n)]^{-1} + [(1/R_{gb}) + j\omega C_{gb}]^{-1} \end{aligned} \quad (2)$$

The term in first bracket gives the complex bulk admittance. The real part of the bulk admittance is then:

$$Y' = (1/R_b) + A\omega^n \quad (3)$$

and the imaginary part of the bulk admittance is

$$Y'' = \omega C_b + B\omega^n \quad (4)$$

One can see the power law dispersion of slope n in the bulk property of the sample both in the real and imaginary parts of the admittance. This analysis shows that, the power law dispersion of the real and imaginary parts of the impedance is the influence of CPE. The distorted arcs in complex modulus planes and the asymmetric peaks in spectroscopic plots of imaginary part of impedance are the effects of this CPE.

We have used commercially available software ZSimpWin to fit the experimentally obtained admittance data with the equivalent circuits suggested before. Figure 5 presents the examples of fits at two temperatures for NPNWTN and NPSWTN. The power law parameter n obtained for both the samples at temperatures below and above transition temperature is listed in Table 1. As CPE contains both real ($A\omega^n$) and imaginary ($jB\omega^n$) parts, it has both resistive and capacitive components. For $n = 1$ CPE reduces to a simple capacitor, and for $n = 0$ it reduces to a simple resistor [26]. Since the fitted data for n has the values between 0 and 1, CPE has both resistive and capacitive components. For the temperatures below transition temperature (T_c), higher values of n suggest CPE for the sample is predominately capacitive (with significant resistive component), whereas above transition temperature, CPE is predominately resistive (with significant capacitive component). This helps us

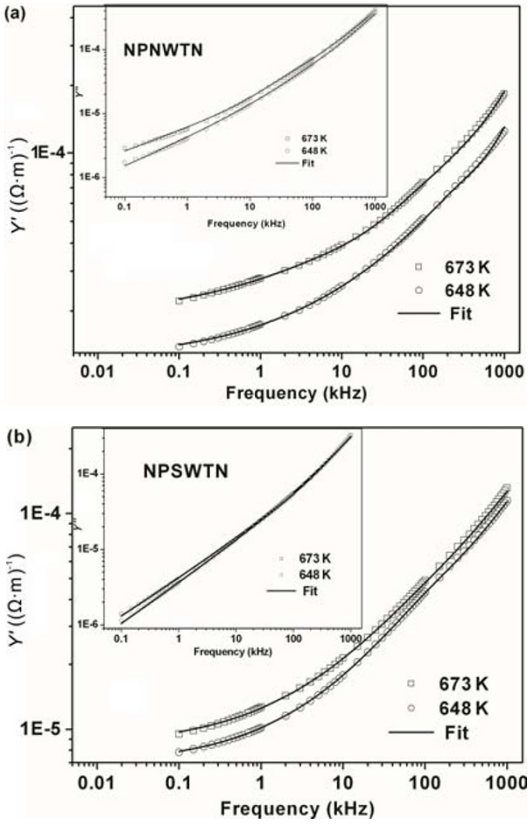

Fig. 5 Spectroscopic plots of complex admittance data (real and imaginary parts) at two different temperatures for (a) NPNWTN and (b) NPSWTN. Solid lines represent fitted data.

Table 1 Values of Y_0 and n for NPSWTN and NPNWTN at different temperatures

Temperature (K) and circuit model	NPNWTN		NPSWTN	
	Y_0	n	Y_0	n
473(R–CPE–C)	9.537×10^{-9}	0.4985	1.942×10^{-9}	0.5433
498(R–CPE–C)	2.427×10^{-8}	0.4951	5.594×10^{-9}	0.5741
523(R–CPE–C)	4.205×10^{-8}	0.5033	1.270×10^{-8}	0.6079
548(R–CPE–C)	6.902×10^{-8}	0.5115	1.997×10^{-8}	0.6102
573(R–CPE–C)(R–C)	1.634×10^{-7}	0.5228	9.354×10^{-8}	0.4957
598(R–CPE–C)(R–C)	1.663×10^{-7}	0.5365	8.077×10^{-8}	0.4884
623(R–CPE–C)(R–C)	1.570×10^{-7}	0.5395	4.479×10^{-8}	0.4772
648(R–CPE–C)(R–C)	4.635×10^{-8}	0.5316	1.289×10^{-7}	0.4279
673(R–CPE–C)(R–C)	7.647×10^{-8}	0.4963	1.608×10^{-7}	0.3703

to infer that n gives a measure of the effectiveness in the dipolar interactions, which is reduced after transition temperature. So our study supports the assumption of Maso *et al*. [26] that CPE is related with the cooperative dipole interactions in the compound.

3.2 Electrical conductivity

From the AC conductivity study, one can get sizable information regarding the nature of charge carriers and the conduction mechanism in the material. The AC conductivity of the sample is given by the relation:

$$\sigma_{\mathrm{AC}} = \varepsilon_{\mathrm{r}}\varepsilon_0\omega\tan\delta \tag{5}$$

where ε_{r} is the dielectric constant; ε_0 is the vacuum permittivity; ω is the angular frequency; and $\tan\delta$ is the loss tangent factor. This AC conductivity for the real dispersive materials depends on the frequency. The functional dependence of AC conductivity on frequency is suggested by Jonscher [10] in the form of a universal power law relation given by

$$\sigma_{\mathrm{AC}}(\omega) = \sigma_0 + A\omega^n \tag{6}$$

where σ_0 is the frequency independent part of the total conductivity called as the DC conductivity. The pre-factor "A" and the exponent "n" are dependent on material and temperature. The dispersion mechanism in the conductivity of the material is measured by the term "$A\omega^n$". The value of n decides the type of charge transport. For $n<1$, the charge carriers are assumed to be taking a translational motion with sudden hopping [27], whereas $n>1$ would mean a localized hopping of the species with a small hopping without leaving the neighborhood [28].

The dependence of AC conductivity on frequency, taken at different temperatures for both the compounds is shown in Fig. 6. The change of conductivity with frequency and temperature can be clearly seen from the plots. At a particular temperature, the conductivity increases with increase in frequency. Also for a particular frequency, the conductivity increases with increase in temperature. This shows that the variation of AC conductivity is a thermally activated process. At low temperatures, in both the materials, the conductivity shows characteristic ω^n dependence. But at high temperatures, the conductivity shows a flat response at low frequency while ω^n dependence is still retained at high frequency. The flat response at high

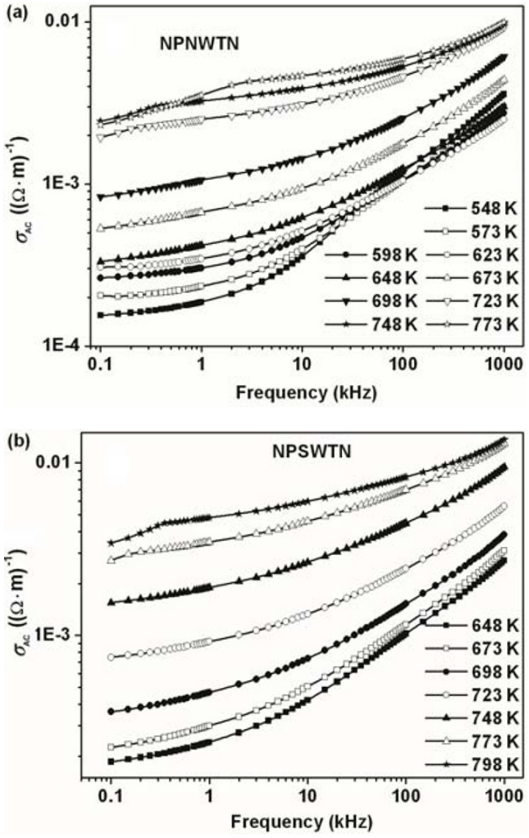

Fig. 6 Variations of AC conductivity σ_{AC} with frequency for (a) NPNWTN and (b) NPSWTN at different temperatures.

temperature and low frequency is attributed to transition from long range hopping to short range ion motion and conductivity relaxation phenomena, whereas the ω^n dependence of σ_{AC} at low frequency in low temperature region is attributed to the space charge polarization. The narrowing of conductivity graphs at high temperature and high frequency is due to the release of space charges. The significant conductivity of the materials is assumed to be due to the higher defect concentration, mainly because of oxygen vacancies.

The conductivity of ionic conducting materials has a significant component contributed from the mobile ion concentration and their hopping rate from one localized site to other. If these localized sites (produced because of interstitial or vacancy mechanism) form a continuous connected network in the sample, the mobile ions can move the entire physical dimension of the sample, which results in a DC current conduction, that cannot be easily separated from the direct current resulted from the movement of free carrier concentration under the bias field. The DC current due to hopping transition depends on the hopping probability which is a function of the distance between the hopping sites and the height of the potential barrier that the hopping ion has to overcome. This transition may be a thermally activated one thereby jumping over the potential barrier or may occur due to tunneling through the potential barrier. The activation energy needed for these two phenomena are largely different, the former being higher and the latter being very small [29].

In ionic conducting materials, the ion hopping rate is mostly thermally assisted and is given by the equation:

$$\omega_p = (\sigma_0 / A)^{1/n} \quad (7)$$

where σ_0, A and n are the DC conductivity, the pre-factor and the exponential factor, respectively. The values of σ_0, A and n can be obtained by fitting AC conductivity data with power law Eq. (6) at high frequency and the values of ω_p at different temperatures are obtained from Eq. (7). Figure 7 shows the variation of $\log\omega_p$ with temperature for both NPNWTN and NPSWTN, which shows nearly linear response with temperature showing Arrhenius variation. The ion hopping rate ω_p is also given by

$$\omega_p = \omega_e \exp[-H_m/(kT)] \quad (8)$$

So

$$\log\omega_p = \log\omega_e - H_m/(kT) \quad (9)$$

where ω_e is the characteristic frequency; H_m is the activation enthalpy; k is the Boltzmann constant; and T is the absolute temperature.

From the slope of the linear fit of $\log\omega_p$ vs. temperature, one can estimate the activation enthalpy. The activation enthalpies for NPNWTN and NPSWTN are calculated to be 1.02 eV and 1.03 eV, respectively. These values are very high compared to activation energy calculated from variation of relaxation time with temperature. This shows that the conduction in the material is due to tunneling through the potential barrier instead of jumping over it.

From the hopping rate, the charge carrier concentration term K' can be easily determined by using the relation [30]:

$$K' = \sigma_0 T/\omega_p \quad (10)$$

Figure 7 (insets) shows the variation of charge carrier concentration with temperature for NPNWTN and NPSWTN. The charge carrier concentration for both the samples is almost constant in the studied temperature range. Hence it is concluded that the increase in conductivity with temperature is thermally

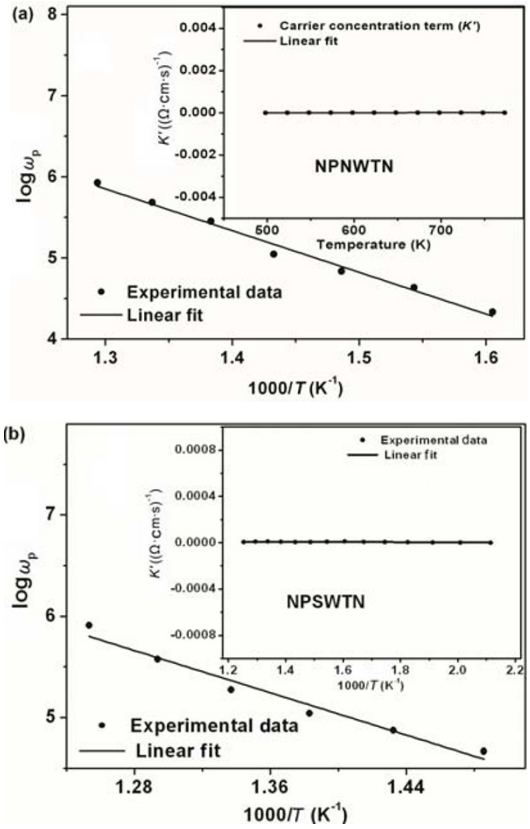

Fig. 7 Variations of hopping rate (ω_p) and charge carrier concentration term (K') with temperature for (a) NPNWTN and (b) NPSWTN.

assisted without any effective increase in charge carrier concentration in the materials.

4 Conclusions

The frequency dependent electrical properties of NPNWTN and NPSWTN were studied successfully using modulus, admittance and AC conductivity formalisms. Electrical response of the compounds at different temperatures was modeled by equivalent circuit(s) consisting of a parallel combination of resistor, CPE and capacitor. Temperature dependent polydispersive relaxation of non-Debye type was observed in both the materials. Variation of relaxation time obtained from loss modulus spectrum showed Arrhenius behavior from which the activation energies for NPNWTN and NPSWTN were calculated to be 0.69 eV and 0.43 eV, respectively. A dominating hopping mechanism in the electrical transport processes for both the compounds was seen from modulus analysis. Variation of power law parameter (n) of CPE with temperature suggested that, CPE represents a cooperative dipolar interaction with increasing capacitive component as the transition temperature is approached, which reduces above T_c, resulting reduction in effectiveness of the dipolar interaction. High frequency AC conductivity data at different temperatures were fitted with Jonscher's power law, and the values of σ_0, A and n were estimated. Hopping rates at different temperatures obtained using Almond and West formalism were found to be obeying Arrhenius behavior, and activation enthalpies were calculated to be 1.02 eV for NPNWTN and 1.03 eV for NPSWTN. The constancy of charge carrier concentration term in the studied temperature range suggested that the conduction process in both the compounds is dominated by thermally assisted hopping conduction mechanism.

References

[1] Rubin JJ, Van Uitert LG, Levinstein HJ. The growth of single crystal niobates for electro-optic and non-linear applications. *J Cryst Growth* 1967, **1**: 315–317.

[2] Stenger CGF, Burggraaf AJ. Study of phase transitions and properties of tetragonal (Pb, La)(Zr, Ti)O_3 ceramics—III: Transitions induced by electric fields. *J Phys Chem Solids* 1980, **41**: 31–41.

[3] Behera B, Nayak P, Choudhary RNP. Structural, dielectric and electrical properties of $NaBa_2X_5O_{15}$ (X = Nb and Ta) ceramics. *Mater Lett* 2005, **59**: 3489–3493.

[4] Mohanty BB, Sahoo PS, Sahoo MPK, *et al*. Structural and electrical properties of $Ba_3Sr_2GdTi_3V_7O_{30}$. *Adv Mat Lett* 2012, **3**: 305–308.

[5] Chen XM, Sun YH, Zheng XH. High permittivity and low loss dielectric ceramics in the $BaO–La_2O_3–TiO_2–Ta_2O_5$ system. *J Eur Ceram Soc* 2003, **23**: 1571–1575.

[6] Fang L, Chen L, Zheng H, *et al*. Structural and dielectric properties of $Ba_5LnSn_3Nb_7O_{30}$ (Ln = La, Nd) ceramics. *Mater Lett* 2004, **58**: 2654–2657.

[7] Behera B, Nayak P, Choudhary RNP. Study of complex impedance spectroscopic properties of $LiBa_2Nb_5O_{15}$ ceramics. *Mater Chem Phys* 2007, **106**: 193–197.

[8] Macdonald JR. *Impedance Spectroscopy*. New York: Wiley, 1987.

[9] Almond DP, West AR. Impedance and modulus spectroscopy of "real" dispersive conductors. *Solid State Ionics* 1983, **11**: 57–64.

[10] Jonscher AK. The 'universal' dielectric response. *Nature* 1977, **267**: 673–679.

[11] Ngai KL, White CT. Frequency dependence of dielectric loss in condensed matter. *Phys Rev B* 1979, **20**: 2475.

[12] Dissado LA, Hill RM. Non-exponential decay in dielectrics and dynamics of correlated systems. *Nature* 1979, **279**: 685–689.

[13] West AR, Sinclair DC, Hirose N. Characterization of electrical materials, especially ferroelectrics, by impedance spectroscopy. *J Electroceram* 1997, **1**: 65–71.

[14] Abouzari MRS, Berkemeier F, Schmitz G, *et al*. On the physical interpretation of constant phase elements. *Solid State Ionics* 2009, **180**: 922–927.

[15] Kaplan T, Gray LJ, Liu SH. Self-affine fractal model for a metal-electrolyte interface. *Phys Rev B* 1987, **35**: 5379.

[16] Maitra MG, Sinha M, Mukhopadhyay AK, *et al*. Ion-conductivity and Young's modulus of the polymer electrolyte PEO–ammonium perchlorate. *Solid State Ionics* 2007, **178**: 167–171.

[17] Zhang Y, Huang Y, Wang L. Study of EVOH based single ion polymer electrolyte: Composition and microstructure effects on the proton conductivity. *Solid State Ionics* 2006, **177**: 65–71.

[18] Das PR, Choudhary RNP, Samantray BK. Diffuse ferroelectric phase transition in $Na_2Pb_2Sm_2W_2Ti_4Nb_4O_{30}$ ceramics. *Mater Chem Phys* 2007, **101**: 228–233.

[19] Das PR, Choudhary RNP, Samantray BK. Diffuse ferroelectric phase transition in $Na_2Pb_2Nd_2W_2Ti_4Nb_4O_{30}$ ceramic. *J Alloys Compd* 2008, **448**: 32–37.

[20] Hodge IM, Ingram MD, West AR. Impedance and modulus spectroscopy of polycrystalline solid electrolytes. *J Electroanal Chem Interfacial Electroch* 1976, **74**: 125–143.

[21] Irvine JTS, Sinclair DC, West AR. Electroceramics: Characterization by impedance spectroscopy. *Adv Mater* 1990, **2**: 132–138.

[22] Das PS, Chakraborty PK, Behera B, *et al*. Electrical properties of $Li_2BiV_5O_{15}$ ceramics. *Physica B* 2007, **395**: 98–103.

[23] Rao KS, Krishna PM, Prasad DM, *et al*. Modulus spectroscopy of lead potassium titanium niobate ($Pb_{0.95}K_{0.1}Ti_{0.25}Nb_{1.8}O_6$) ceramics. *J Mater Sci* 2007, **42**: 4801–4809.

[24] Ngai RL, León C. Recent advances in relating macroscopic electrical relaxation data to microscopic movements of the ions in ionically conducting materials. *Solid State Ionics* 1999, **125**: 81–90.

[25] Barker AS, Ditzenberger JA, Remeika JP. Lattice vibrations and ion transport spectra in β-alumina. II. Microwave spectra. *Phys Rev B* 1976, **14**: 4254.

[26] Masó N, Yue XY, Goto T, *et al*. Frequency-dependent electrical properties of ferroelectric $BaTi_2O_5$ single crystal. *J Appl Phys* 2011, **109**: 024107.

[27] Funke K. Jump relaxation in solid electrolytes. *Prog Solid State Ch* 1993, **22**: 111–195.

[28] Sen S, Choudhary RNP. Impedance studies of Sr modified $BaZr_{0.05}Ti_{0.95}O_3$ ceramics. *Mater Chem Phys* 2004, **87**: 256–263.

[29] Zheludev IS. *Physics of Crystalline Dielectrics. Vol. 2 Electrical Properties*. New York–London: Plenum Press, 1971.

[30] Varada Rajulu KC, Tilak B, Rao KS. Electricalconductivity and dielectric properties of $Bi_{0.5}(Na_{0.7}K_{0.2}Li_{0.1})_{0.5}TiO_3$ ceramic material. *American Journal of Materials Science* 2012, **2**: 15–21.